

Scaling and self-similarity for the dynamics of a particle confined to an asymmetric time-dependent potential well

Diogo R. da Costa,^{1,2} J. A. Méndez-Bermúdez,³ and Edson D. Leonel¹

¹*Departamento de Física, UNESP - Universidade Estadual Paulista - Av. 24A, 1515, Bela Vista, CEP: 13506-900 Rio Claro, SP, Brazil*

²*Departamento de Matemática e Estatística - UEPG, 84030-000 Ponta Grossa, PR, Brazil*

³*Instituto de Física, Benemérita Universidad Autónoma de Puebla, Apartado Postal J-48, 72570 Puebla, México*



(Received 24 May 2018; published 2 January 2019)

The dynamics of a classical point particle confined to an asymmetric time-dependent potential well is investigated under the framework of scaling. The potential corresponds to a reduced version of a particle moving along an infinitely periodic sequence of synchronously oscillating potential barriers. The dynamics of the model is described by a two-dimensional nonlinear and area preserving map in energy and phase variables. The asymmetric potential well is defined by two regions: Region I with fixed null potential and region II with an oscillating potential. The time-dependent potential of region II makes, for certain initial conditions, the particle to undergo a number of multiple reflections η at the border of the two regions and stay trapped in region I. Such trappings are described by histograms of multiple reflections η , obeying the power-law $H(\eta) \propto \eta^{-\nu}$ with $\nu \approx 3$, which are scale invariant with a scaling parameter depending of the control parameters of the mapping. We identify the location of the sets of initial conditions in phase space producing the multiple reflections and show that they generate well defined self-similar structures in density plots of trajectories in energy space. The self-similar structures can be enhanced by properly tuning the system parameters.

DOI: [10.1103/PhysRevE.99.012202](https://doi.org/10.1103/PhysRevE.99.012202)

I. INTRODUCTION

Particles moving along potential wells or potential barriers are paradigmatic systems in classical mechanics, quantum mechanics, and electrodynamics; for recent studies see Refs. [1–8]. This class of systems can be described by the use of different procedures that may range from quantum approaches, where the Schrödinger equation is solved, to classical-chaos investigations, where chaotic seas are characterized by Lyapunov exponents, passing through the description of phase transitions with the variation of control parameters, among other approaches [9–14]. The effect of noise in the dynamics and other kinds of perturbations are also subjects of interest [12]. In the classical case and considering time perturbations to the potential, the particles may exhibit chaotic motion leading to scaling invariance under the variation of control parameters whenever also the escape of particles from specific regions of the phase space can be considered [12,14]. To cite an application of the quantum case, the Gaussian wave-packet dynamics and quantum tunneling in asymmetric double-well systems were reported in [15].

The model considered in this paper is a classical particle, or equivalently an ensemble of noninteracting particles, confined to move inside a potential box which contains a periodically oscillating time-dependent barrier. The Hamiltonian that describes the model is of the type $H(x, p, t) = p^2/(2\mu) + V(x, t)$, where x , p , and t correspond to the position, momentum, and time, respectively. The potential $V(x, t)$ is controlled by dimensionless parameters. A phase transition from integrability—characterized by a constant energy of the particle—to non-integrability, where the particle may develop either chaotic or regular dynamics, is observed when changing the control parameters. The dynamics

of the model is described by a two-dimensional non-linear area preserving mapping, for the variables energy and time. The phase space of the model is of mixed type and shows periodic islands surrounded by a chaotic sea limited by a set of invariant spanning curves preventing unlimited diffusion in energy. Applications of the formalism are immediate since for some materials, like photonic crystals, the heterostructure can be conveniently considered as a chain with an infinite number of time-dependent potential barriers (or wells), as shown in Fig. 1(a). These potential barriers can also be the representation of quantum dots [16,17]. In our system, the top of the barriers are oscillating in synchrony, where it can happens, for example, due to the electron-phonon interaction [18] or the presence of a monochromatic electromagnetic or acoustic field [19,20]. Considering the barriers are symmetric, one can map the infinite sequences of barriers to a single time-dependent barrier, as shown in Fig. 1(b).

This paper is organized as follows. In Sec. II we describe in detail the construction of the two-dimensional nonlinear mapping used in the study of the dynamics of particles confined into the asymmetric time-dependent potential well. Also we define the main quantity of investigation: the number of multiple reflections η that particles, having specific initial conditions, suffer at the interface of the two regions defining the asymmetric potential well. Such multiple reflections are naturally observed in the chaotic dynamics, however are rare as compared to the whole dynamics. The results and discussion are presented in Secs. III and IV: First we perform a scaling analysis of the histograms of η (Sec. III) and then show the emergence of self-similar structures in energy space (Sec. IV). Finally, a summary is given in Sec. V.

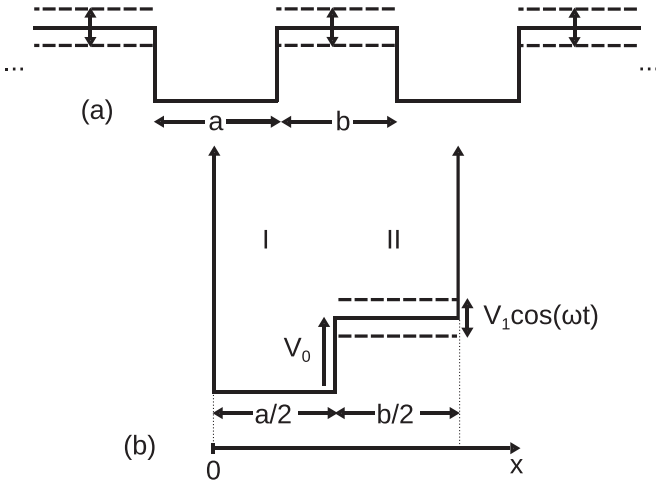


FIG. 1. (a) Sketch of an infinite sequence of identical potential barriers whose height oscillates periodically in time. (b) Time-dependent potential well corresponding to the desymmetrized version of the sequence of potential barriers in (a). I and II label the two regions of the well. a , b , V_0 , V_1 , and ω are the control parameters of the dynamical system.

II. DYNAMICAL MODEL AND CORRESPONDING MAPPING

We consider a classical particle of mass μ that moves along an infinite sequence of identical potential barriers of width b whose height oscillates periodically in time as shown in Fig. 1(a). The barriers are separated by a distance a from each other. Since the potential is periodic we can focus on its desymmetrized version; that is, we shall study the dynamics of the potential depicted in Fig. 1(b) which is given by

$$V(x, t) = \begin{cases} \infty, & x \leq 0, \\ 0, & 0 < x < a/2, \\ V_0 + V_1 \cos(\omega t), & a/2 \leq x < (a+b)/2, \\ \infty, & (a+b)/2 \leq x. \end{cases} \quad (1)$$

Here, V_0 , V_1 , and ω are, respectively, the average barrier height, the barrier height oscillation amplitude, and the oscillation frequency. Therefore, a , b , V_0 , V_1 , and ω are the control parameters of the system. Similar wells have been studied in Refs. [12,14,20]; none of those works considered the investigation we are dealing with in this paper. Also, we have defined two regions in the well, labeled as I and II in Fig. 1(b).

We describe the dynamics of a particle inside the well of Fig. 1(b) by the use of a mapping. To construct the mapping we consider a particle (at time $t = t_n$) with energy given by

$$E_n > V_0 + V_1 \cos(\omega t_n), \quad (2)$$

immediately before entering region I (at $x = a/2$) from region II. We define position $x = a/2$ as a Poincaré section, so the mapping is iterated each time the particle reaches that point. After entering in region I the particle suffers an abrupt change in its kinetic energy, $K \equiv \mu v^2/2$, but due to total energy

conservation

$$K'_n = E_n. \quad (3)$$

Once in region I the particle moves to the left with constant velocity $v'_n = \sqrt{2K'_n/\mu}$, since there are no forces acting on it. The particle travels until it reaches the infinitely-high potential barrier at $x = 0$. It is reflected backwards and travels to the right up to $x = a/2$ with an energy given by

$$E'_n = K'_n. \quad (4)$$

The time to travel the distance a is $\Delta t_a = a/v'_n$. At $x = a/2$ two different situations may happen: (i) The particle has not enough energy to leave region I, or (ii) the particle enters in region II. Case (i) is observed for

$$E'_n \leq V_0 + V_1 \cos[\omega(t_n + \Delta t_a)],$$

at which the particle suffers a reflection, staying in region I. So it travels again to the left, reaches the infinite potential at $x = 0$, it is reflected there and returns to $x = a/2$. The condition to leave region I, therefore leading to Case (ii), is

$$E'_n > V_0 + V_1 \cos[\omega(t_n + i \Delta t_a)], \quad (5)$$

where i is the smallest integer number that satisfies Eq. (5). For $i = 1$ the particle does not stay trapped in region I, leaving it immediately after one full incursion. For $i = 2$ the particle suffers only one reflection at $x = a/2$ and leaves region I after two full incursions. $i = 3$ corresponds to a particle leaving region I after three full incursions and so on. Therefore, the number of successive reflections of the particle at $x = a/2$, without leaving region I, is given by

$$\eta = i - 1. \quad (6)$$

We stress that in the following sections we will focus our study on the quantity η .

If condition (5) is satisfied, the particle has enough energy to leave region I. It then suffers another abrupt change in its kinetic energy

$$K''_n = E'_n - \{V_0 + V_1 \cos[\omega(t_n + i \Delta t_a)]\}.$$

The particle travels the distance b , which takes a time $\Delta t_b = b/v''_n$, with constant velocity given by $v''_n = \sqrt{2K''_n/\mu}$. After that the particle reaches the Poincaré section just before entering into region I again. There, at $x = a/2$, the energy is

$$E_{n+1} = K''_n + V_0 + V_1 \cos(\omega t_{n+1}), \quad (7)$$

at time

$$t_{n+1} = t_n + i \Delta t_a + \Delta t_b. \quad (8)$$

Rewriting the two expressions we obtain the mapping

$$T : \begin{cases} E_{n+1} = E_n + V_1 [\cos(\omega t_{n+1}) - \cos(\omega(t_n + i \Delta t_a))] \\ t_{n+1} = t_n + i \Delta t_a + \Delta t_b, \quad \text{mod}(2\pi/\omega) \end{cases}. \quad (9)$$

In order to reduce the number of control parameters of mapping (9) it is convenient to consider the following set of dimensionless variables: $e = E/V_0$, $\phi = \omega t$, $\Delta\phi_a = \omega \Delta t_a$, and $\Delta\phi_b = \omega \Delta t_b$. The control parameters of the dynamical

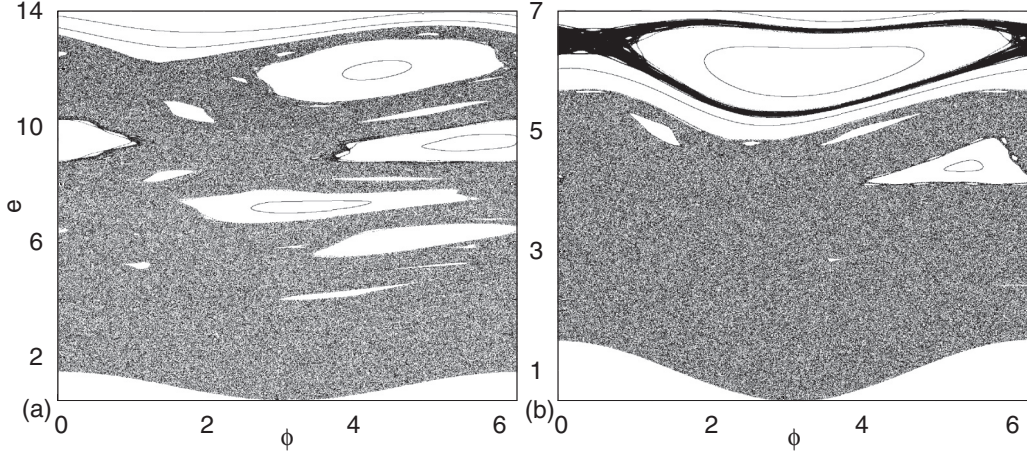


FIG. 2. Phase space portraits e vs. ϕ for mapping (11). The parameters considered are: (a) $(N_c, r, \delta) = (100, 0.5, 0.5)$ and (b) $(N_c, r, \delta) = (30, 1, 0.5)$.

system become

$$\delta = \frac{V_1}{V_0}, \quad r = \frac{b}{a}, \quad \text{and} \quad N_c = a \sqrt{\frac{\mu}{2V_0}} \omega. \quad (10)$$

The parameter δ controls the height of the potential barrier, r characterizes its width, and N_c is the normalized oscillation frequency of the barrier. We note that for $\delta = 0$ or $N_c = 0$ the system is integrable (no chaotic structures can be observed).

Using the new variables, the mapping T gets the form

$$T : \begin{cases} e_{n+1} = e_n + \delta[\cos(\phi_{n+1}) - \cos(\phi_n + i\Delta\phi_a)] \\ \phi_{n+1} = \phi_n + i\Delta\phi_a + \Delta\phi_b, \quad \text{mod}(2\pi) \end{cases}, \quad (11)$$

where

$$\Delta\phi_a = \frac{N_c}{\sqrt{e_n}}, \quad (12)$$

and

$$\Delta\phi_b = \frac{N_c r}{\sqrt{e_n - 1 - \delta \cos(\phi_n + i\Delta\phi_a)}} \quad (13)$$

are auxiliary dimensionless variables which, respectively, measure the time to travel the distances a and b .

Typical phase portraits (e vs. ϕ) for the mapping (11) are shown in Fig. 2. The phase space is of mixed type containing periodic islands, chaotic regions, and invariant spanning curves limiting the size of the chaotic sea preventing unlimited diffusion of energy and separating different regions of chaos. Depending on the combination of control parameters the position of the lowest invariant spanning curve changes. Also note that the phase portraits are bounded from below by the curve $e = 1 + \delta \cos(\phi)$, defining the border of allowed energies of Eq. (2).

Once the mapping describing the dynamics is constructed, allowing easy computation of the orbits, we then concentrate on the quantity η . Thus, in the following section we study scaling properties of η .

III. SCALING OF THE NUMBER OF SUCCESSIVE REFLECTIONS

As previous results in literature reported for other models, we expect scaling invariance of the quantity η (see for example Refs. [21] and [22] where scaling properties of multiple reflections of light beams inside a modulated waveguide and of particles trapped in an oval billiard were investigated).

We start the scaling analysis of η by constructing histograms, $H(\eta)$, for different values of the parameter N_c . Without loss of generality we fix the values of r and δ to 1 and 0.5, respectively. In Fig. 3(a) we show $H(\eta)$ for $N_c = 30$, $N_c = 400$, and $N_c = 4000$ [here, $N_c = 30$ corresponds to the phase portrait of Fig. 2(b)]. To construct each histogram a single trajectory with the initial condition $\phi_0 = 1.23$ and $e_0 = [1 + \delta \cos(\phi_0) + 10^{-3}]$ was iterated 10^{10} times.

Notice the histograms in Fig. 3(a) show a clear power-law decay,

$$H(\eta) \propto \eta^{-\nu_1}, \quad (14)$$

for large η . Also note that ν_1 is very close to 3 and does not seem to depend on the values of the control parameters (not shown here in full detail). From this figure, one can also observe that the histograms are displaced to the left for increasing N_c showing a typical scaling behavior. To look at the scaling we first define a quantity that can quantify the displacement of the histograms produced by changing N_c . Indeed, we choose the value of η such that $H(\eta) \approx 10^4$; i.e., the intersection of the histograms with the horizontal line at $H(\eta) = 10^4$, see the dashed line in Fig. 3(a). Thus, in Fig. 3(b) we plot η , for $H(\eta) \approx 10^4$, for several values of $N_c \in [30, 10^4]$ and observe a clear power-law behavior of the form

$$\eta[H(\eta) \approx 10^4] \propto N_c^{-\nu_2}, \quad (15)$$

with $\nu_2 = 0.218(2)$.

Therefore, in Fig. 3(c) we plot again the histograms of Fig. 3(a) but now as a function of the scaling parameter $\eta \times N_c^{\nu_2}$. A clear overlap of all histograms onto a unique universal curve is observed, which verifies the scaling of $H(\eta N_c^{\nu_2})$.

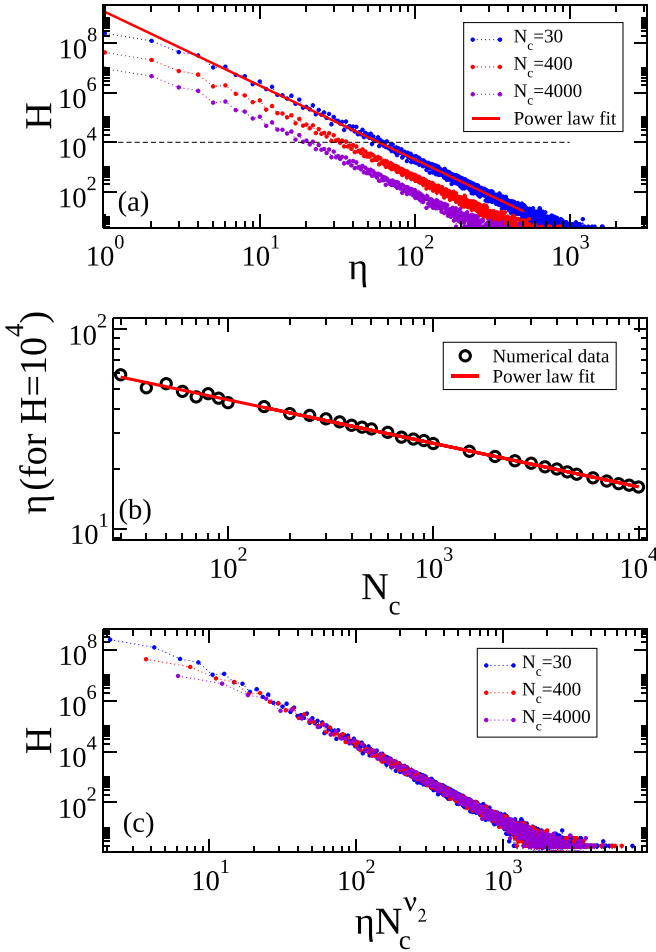


FIG. 3. Plot of (a) histograms $H(\eta)$ of the number of successive reflections at $x = a/2$, see Fig. 1(b); the parameters used were $N_c = 30$, $N_c = 400$, and $N_c = 4000$ for fixed $r = 1$ and $\delta = 0.5$. Each histogram was constructed by iterating 10^{10} times a single trajectory with initial condition $\phi_0 = 1.23$ and $e_0 = [1 + \delta \cos(\phi_0) + 10^{-3}]$. The red full line corresponds to a power-law fit with Eq. (14) with $\nu_1 = 2.97(1)$. The dashed line at $H(\eta) = 10^4$ is shown to guide the eye, see the text. (b) η , at $H(\eta) \approx 10^4$, as a function of N_c . The red full line corresponds to a power-law fit with Eq. (15) with $\nu_2 = 0.218(2)$. (c) Histograms $H(\eta)$ of (a) but now as a function of the scaling parameter $\eta \times N_c^{\nu_2}$.

Even though showing that histograms of the number of successive reflections of particles obey a scaling law is already an important result, since it shows universality in the dynamics of the model, we want to go one step further and explore the rich structure that successive reflections produce when analyzing their location in phase space.

IV. LOCATION OF SUCCESSIVE REFLECTED TRAJECTORIES IN PHASE SPACE

The function $\text{mod}(2\pi)$ in map (11) makes the phase ϕ_{n+1} to lie in the interval $[0, 2\pi)$ therefore in a cylindrical symmetry. If the mod function is not applied, ϕ_{n+1} becomes unbounded in the phase orientation. In such a case, we define

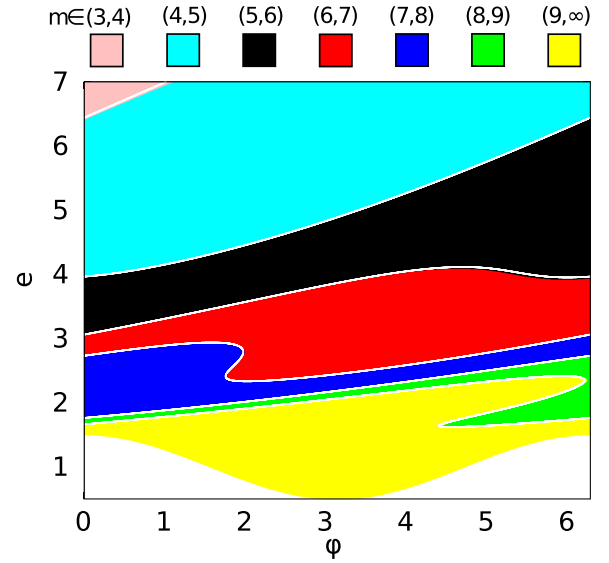


FIG. 4. Color map of m on the phase portrait of Fig. 2(b); i.e., for $(N_c, r, \delta) = (30, 1, 0.5)$. Here, $\eta = 0$ was considered.

m as the magnitude of ϕ_{n+1} given in units of 2π :

$$m = \frac{\phi_{n+1}}{2\pi}. \quad (16)$$

Note that m measures the spread of ϕ in the phase axis. From Eq. (11), given the pair (ϕ_n, e_n) , the phase $\phi_{n+1} \equiv 2\pi m$ can be written as

$$2\pi m = \phi_n + \frac{iN_c}{\sqrt{e_n}} + \frac{N_cr}{\sqrt{e_n - 1 - \delta \cos\left[\phi_n + i\frac{N_c}{\sqrt{e_n}}\right]}}, \quad (17)$$

from which m can be computed. In Fig. 4 we show a color map of m on the phase portrait of Fig. 2(b). In this figure we report the phase-space regions corresponding to $m \in (3, \infty)$, moreover we are grouping $m \in (9, \infty)$ in the yellow region located at low energies. Notice that different colors in Fig. 4 are separated by white stripes which represent integer values of m ; there, the white stripes correspond to $m = 4, 5, 6, 7, 8, 9$ from top to bottom. It is important to stress that the color map of Fig. 4 was obtained for $\eta = 0$ only, i.e., from particle trajectories leaving region I immediately after one full incursion. To complete Fig. 4, in Fig. 5(a) we show the curves in phase space produced by integer values of $m \geq 9$. Note that the curves for increasing m converge to limiting curves. Clearly, those limiting curves define blank regions in the phase space of Fig. 5(a). Moreover, such “blank regions” contain the information of the multiple reflected trajectories characterized by $\eta > 0$. To explicitly show this, in Fig. 5(b) we present a color map of the regions corresponding to values of $\eta > 0$. Also, to better show details, in Fig. 5(c) we present the enlargement of the dashed box of Fig. 5(b).

In fact, the scenario reported in Figs. 5(a)–5(c) can be well described by Eq. (17): We first take the limit $m \rightarrow \infty$ in Eq. (17) to obtain

$$e - 1 - \delta \cos\left[\phi + i\frac{N_c}{\sqrt{e}}\right] = 0, \quad (18)$$

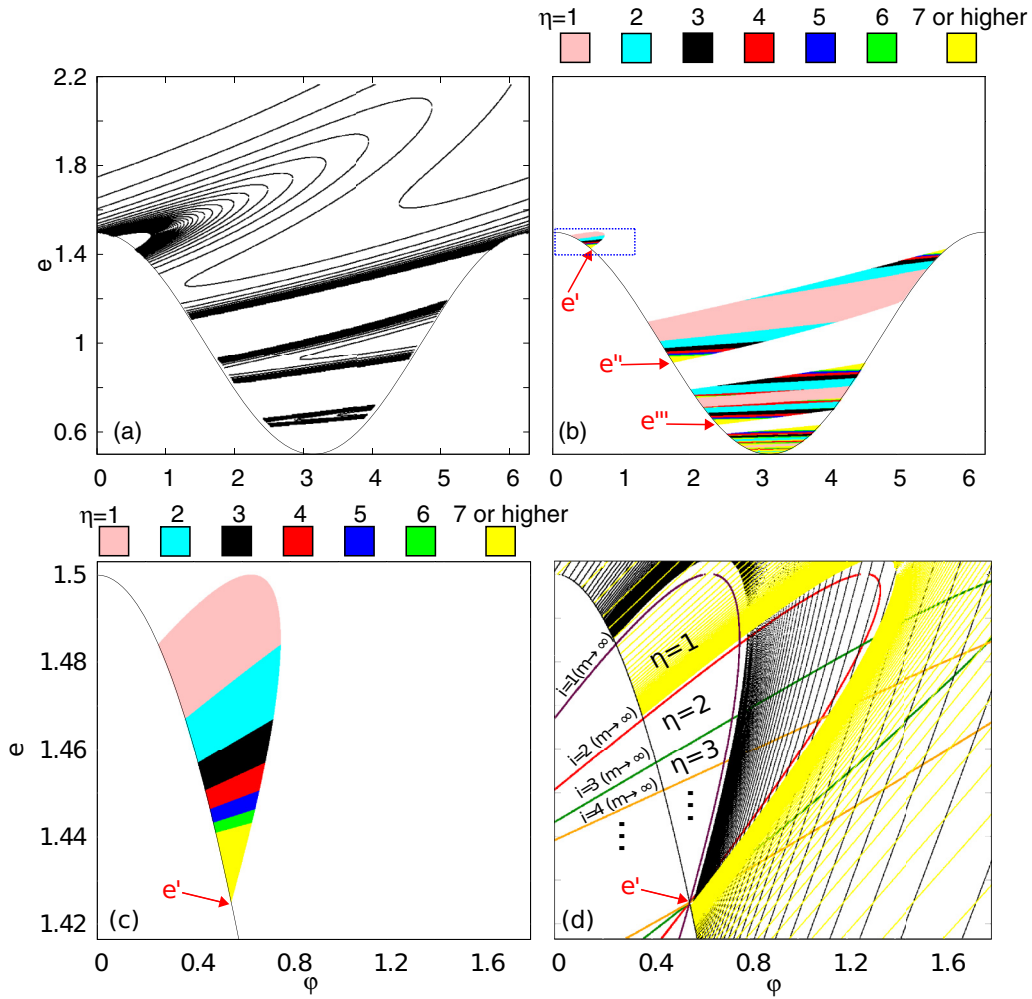


FIG. 5. (a) Curves for integer values of $m \geq 9$. As well as in Fig. 4, $\eta = 0$ was considered here. (b) Color map of m for $\eta \geq 1$. (c) Enlargement of the blue dashed box in (b). (d) Curves produced by Eqs. (19) or (20), i.e., for $m \rightarrow \infty$, for different values of $i \geq 1$. $(N_c, r, \delta) = (30, 1, 0.5)$ in all panels.

which leads us to

$$\phi = \arccos\left(\frac{e-1}{\delta}\right) - i \frac{N_c}{\sqrt{e}} \quad (19)$$

or

$$\phi = 2\pi - \arccos\left(\frac{e-1}{\delta}\right) - i \frac{N_c}{\sqrt{e}}. \quad (20)$$

Then, in Fig. 5(d) we plot curves corresponding to $i = 1, 2$, and so on (corresponding to $\eta = 0, 1, \dots$, respectively) in the phase space region of Fig. 5(c). In fact, the curves produced by Eqs. (19) or (20) with $i = 1$ correspond to the converging curves of Fig. 5(a); while curves with $i > 1$ separate the different colored regions in Figs. 5(b) and 5(c). Furthermore, notice in Fig. 5(d) that curves for different η cross in well defined points of phase space that we label as e', e'', e''' , etc.; see Figs. 5(b)–5(d). Indeed, e' , as well as their images e'', e''', \dots , are accumulation points for $i \rightarrow \infty$; i.e., they mark points in phase space corresponding to trajectories that never escape from region I. Below we show that approaching this points reveals a fractal structure.

The self-similar structure of the density of successive reflections

Finally, let us explore the structures revealed in density plots of successive reflected trajectories that we construct as follows: We count the number of trajectories that visit the boxes in a grid of 1000×1000 equally spaced intervals in the $e_1 e_0$ plane when iterating a dense set of 10^{10} initial conditions with map (11). In particular we define the quantity Ψ as the \log_{10} of the number trajectories that visit a given box Σ :

$$\Psi = \log_{10} \Sigma. \quad (21)$$

Here, the log function is used to suppress regions with huge counts. Then, in Fig. 6(a) we present the density plot obtained for Ψ when $(N_c, r, \delta) = (30, 1, 0.5)$. There, we note that a non trivial structure, i.e., self-similar, reveals at low energies; see also Fig. 6(b) and further enlargements in Figs. 6(c) and 6(d).

Moreover, a detailed analysis shows that the first (i.e., the outer) swallow-like layer forming the self-similar structure in Fig. 6(c), with edge at $e_0 \approx 1.4$, is produced by trajectories characterized by $\eta = 1$. The second swallow-like layer with edge at $e_0 \approx 1.1$ is formed by trajectories with $\eta = 2$, the

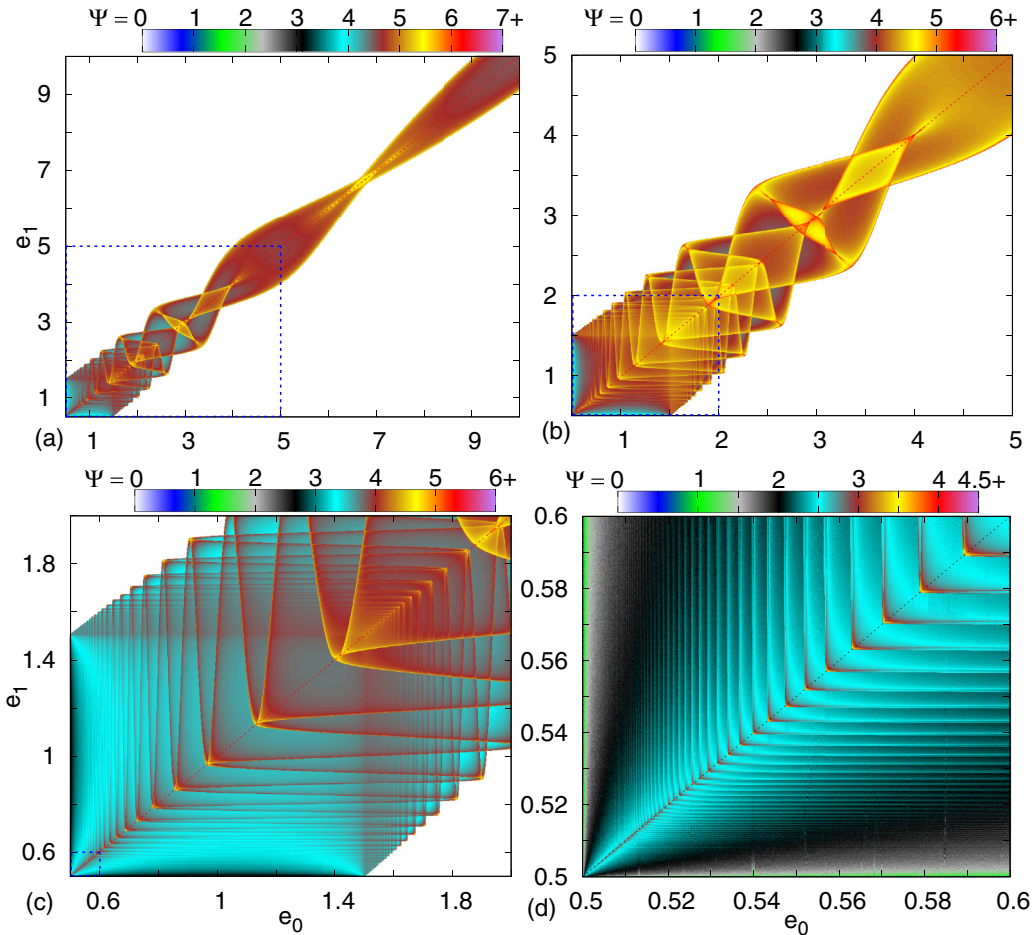


FIG. 6. Density plots of Ψ , as defined in Eq. (21). In (b), (c), and (d) the enlargements of the dashed regions of (a), (b), and (c), respectively, are presented. $(N_c, r, \delta) = (30, 1, 0.5)$ were used.

third layer corresponds to trajectories having $\eta = 3$, and so on. Thus, in Fig. 6(d) the layers with $\eta \geq 12$ are shown; here, the accumulation point at $\eta \rightarrow \infty$ corresponds to $e_0 = 1 - \delta = 0.5$.

It is important to stress that the appearance of the self-similar structure in Fig. 6 does not depend on the choice of parameters made there. Indeed, we detect the appearance of self-similar structures in the $e_0 e_1$ plane when

$$e_0 \in [1 - \delta, 1 + \delta] \quad (22)$$

for any combination of (N_c, r, δ) . That self-similar structures are located in the interval (22) can be well understood since: (i) for $e_0 > 1 + \delta$ particles leave region I without suffering reflections at $x = a/2$ but (ii) $e_0 = 1 - \delta$ is the minimum energy for our dynamical system to work; therefore, $\eta > 0$ requires Eq. (22).

Finally, in Fig. 7 we present additional examples of self-similar structures. There (in left, middle, and right panels, respectively) we used $\delta = 0.25, 0.75$, and 1 (1 is the maximum possible value of δ we can use). Note the larger the value of δ the larger the self-similar structure, as anticipated by condition (22).

It is relevant to mention that self-similar structures, comparable to ours, have been reported in Refs. [23,24]. There, they were produced by whispering gallery orbits (WGO) in

billiards with concave walls. It was also shown [23] that those self-similar structures in the energy space are mapped into self-similar regions in phase-space (something we did not study here). Moreover, since the main focus of Refs. [23,24] was the ray-wave correspondence of scattering quantities, the dependence of self-similar structures with the model parameters was not explored. Thus, we stress that here we are performing a systematic study of the self-similar structures present in our time-dependent potential well and, furthermore, identify the parameter that tune their size; a study that could also be extended to the billiards of Refs. [23,24].

We would like to note that the trapping of particles (due to multiple reflections) in region I of the desymmetrized asymmetric time-dependent potential well, see Fig. 1(b), is equivalent to the trapping of particles in one of the wells of the periodic version of the model, see Fig. 1(a). Thus, the identification of the range of initial energies producing the self-similar structures may be used: (i) To tune the diffusion properties of particles in the periodic version of the potential well. That is, an ensemble of particles with initial energies in the range given by Eq. (22) should diffuse slower (due to trapping) along the periodic potential well than particles with higher energies. (ii) To tune the scattering properties in an *open* version of the periodic time-dependent potential well, i.e., particles injected into a finite version of the

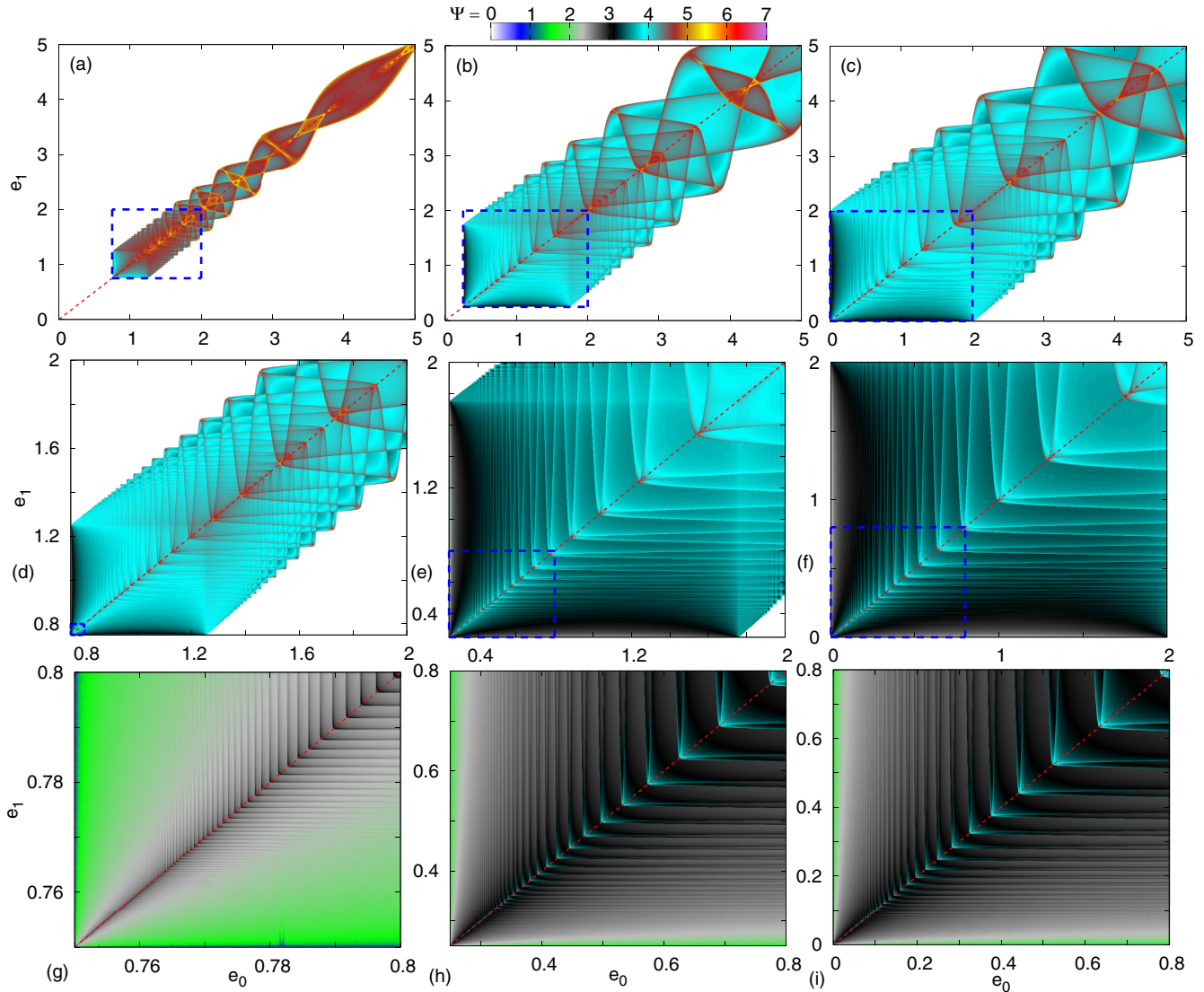


FIG. 7. Density plots of Ψ , as defined in Eq. (21). $(N_c, r) = (100, 0.5)$ and (a), (d) and (g) $\delta = 0.25$, (b), (e) and (h) $\delta = 0.75$, (c), (f) and (i) $\delta = 1$. Panels in second and third rows are enlargements of corresponding panels in the first row.

periodic potential well with energies in the range of Eq. (22) should spend longer times inside the scattering region (due to multiple reflections inside wells) before being reflected or transmitted than particles with higher energies. This is in contrast to the billiards of Refs. [23,24] where the self-similar structures were produced by WGO that, in turn, correspond to trajectories with preferential transmission, i.e., with short delay times. Moreover, as well as in the ray-wave studies of [23,24], we expect the self-similar structures we reported here for the ray version of the model can also be observed in the corresponding quantum or wave version of our time-dependent potential well.

V. SUMMARY

We have performed a detailed numerical study of the dynamics of a classical particle moving along an infinitely periodic sequence of time-dependent potential barriers, whose desymmetrized version is an asymmetric time-dependent

potential well, see Fig. 1. The asymmetric potential well is defined by two regions: region I with fixed null potential and region II with an oscillating potential. This well can be described by a two-dimensional nonlinear mapping in energy and phase variables $T : (e_n, \phi_n) \mapsto (e_{n+1}, \phi_{n+1})$, see Eq. (11). Mapping T has three control parameters: δ , r , and N_c , they control the mean height of the potential barrier, its width, and the oscillation frequency of the moving barrier, respectively; see Eq. (10). Mapping T produces generic mixed phase space portraits having periodic islands, chaotic regions, and invariant spanning curves, see two examples in Fig. 2. The oscillating potential of region II makes the particle to undergo a number of multiple reflections η at the border of the two regions, so the particle stays trapped in region I for a while. By performing a scaling analysis, we showed that histograms of η , which show the power law behavior $H(\eta) \propto \eta^{-\nu_1}$ with $\nu_1 \approx 3$, are scale invariant with the scaling parameter $\eta \times N_c^{\nu_2}$, with $\nu_2 = 0.218(2)$; see Fig. 3. Then, we identify in phase space the sets of initial

conditions producing the multiple reflections, see Figs. 4 and 5.

Finally, we show that multiple reflections generate well defined self-similar structures in density plots of trajectories in energy space, see Fig. 6. Such self-similar structures appear for any combination of parameters (N_c, r, δ) when the initial energy falls in the interval $[1 - \delta, 1 + \delta]$, see Eq. (22) and Fig. 7. Thus, the larger the value of δ (whose maximal value can be one) the larger the region of the self-similar structure in the $e_0 e_1$ space.

It is important to underline that here we focus our attention on (i) the scaling analysis of the histograms of multiple reflections produced by trapped trajectories, and (ii) the identification and characterization of self-similar structures produced by the trajectories wandering in sticky regions of phase space. This may add some insight into the mechanisms that induce the phase-space trapping of trajectories, a subject of interest

in non-linear dynamics since long ago; see for example the reviews of Escande [25] and Zaslavsky [26].

Since similar self-similar structures were also reported in Refs. [23,24], we believe that they may be ubiquitous of dynamical systems and may be observed in regions of the phase space where either temporal or spatial invariance are present.

ACKNOWLEDGMENTS

D.R.C. acknowledges Brazilian agency CAPES-PNPD. This research was supported by resources supplied by the Center for Scientific Computing (NCC/GridUNESP) of the São Paulo State University (UNESP). E.D.L. thanks CNPq (Grant No. 303707/2015-1) and FAPESP (Grant No. 2017/14414-2). J.A.M.-B. acknowledges support from CONACyT (Grant No. CB-2013/220624).

-
- [1] B. Pal, D. Dutta, and S. Poria, *Pramana J. Phys.* **89**, 32 (2017).
 - [2] G. Sulyok, K. Durstberger-Rennhofer, and J. Summhammer, *Phys. Lett. A* **379**, 1699 (2015).
 - [3] S. Longhi and G. DellaValle, *Phys. Rev. A* **87**, 052116 (2013).
 - [4] F. R. N. Koch, F. Lenz, C. Petri, F. K. Diakonov, and P. Schmelcher, *Phys. Rev. E* **78**, 056204 (2008).
 - [5] M. R. A. Shegelski, T. Poole, and C. Thompson, *Eur. J. Phys.* **34**, 569 (2013).
 - [6] V. Dominguez-Rocha and M. Martinez-Mares, *J. Phys. A* **46**, 235101 (2013).
 - [7] M. Diaz, P. A. Mello, M. Yopez, and S. Tomsovic, *Phys. Rev. B* **91**, 184203 (2015).
 - [8] N. P. Mehta, K. R. A. Hazzard, and C. Ticknor, *Phys. Rev. A* **98**, 062703 (2018).
 - [9] G. A. Luna-Acosta, G. Orellana-Rivadeneira, A. Mendoza-Galvan, and C. Jung, *Chaos Solitons Fractals* **12**, 349 (2001).
 - [10] O. Farago and Y. Kantor, *Physica A (Amsterdam)* **249**, 151 (1998).
 - [11] M. Leng and C. S. Lent, *Phys. Rev. Lett.* **71**, 137 (1993).
 - [12] D. R. da Costa, C. P. Dettmann, and E. D. Leonel, *Phys. Rev. E* **83**, 066211 (2011).
 - [13] P. S. S. Guimarães, B. J. Keay, J. P. Kaminski, S. J. Allen, Jr., P. F. Hopkins, A. C. Gossard, L. T. Florez, and J. P. Harbison, *Phys. Rev. Lett.* **70**, 3792 (1993).
 - [14] D. R. da Costa, I. L. Caldas, and E. D. Leonel, *Appl. Math. Comput.* **236**, 215 (2014).
 - [15] H. Hasegawa, *Phys. A* **392**, 6232 (2013).
 - [16] J. Wu, B.-L. Gu, J. Liu, Y. Guo, J.-L. Zhu, J.-Z. Yu, and Y. Kawazoe, *Phys. Lett. A* **262**, 245 (1999).
 - [17] E. D. Leonel and J. K. L. da Silva, *Physica A (Amsterdam)* **323**, 181 (2003).
 - [18] W. Cai, T. F. Zheng, P. Hu, B. Yudanin, and M. Lax, *Phys. Rev. Lett.* **63**, 418 (1989).
 - [19] L. P. Kouwenhoven, S. Jauhar, J. Orenstein, P. L. McEuen, Y. Nagamune, J. Motohisa, and H. Sakaki, *Phys. Rev. Lett.* **73**, 3443 (1994).
 - [20] D. R. da Costa, I. L. Caldas, and E. D. Leonel, *Phys. Lett. A* **377**, 1814 (2013).
 - [21] M. R. Silva, D. R. da Costa, and E. D. Leonel, *J. Phys. A* **45**, 265101 (2012).
 - [22] D. R. da Costa, C. P. Dettmann, J. A. de Oliveira, and E. D. Leonel, *Chaos* **25**, 033109 (2015).
 - [23] J. A. Mendez-Bermudez, G. A. Luna-Acosta, P. Seba, and K. N. Pichugin, *Phys. Rev. E* **66**, 046207 (2002).
 - [24] S. Félix and V. Pagneux, *Wave Motion* **41**, 339 (2005).
 - [25] D. F. Escande, *Phys. Rep.* **121**, 165 (1985).
 - [26] G. M. Zaslavsky, *Phys. Rep.* **371**, 461 (2002).